MEASUREMENTS OF OSCILLATORY DRAG ON SAND RIPPLES

Karl E. B. Lofquist
National Bureau of Standards
Washington, D.C.

ABSTRACT

Measurements have been made of drag on naturally rippled sand beds in an oscillatory-flow water tunnel. A partition splits the tunnel into two parallel channels with equal cross sections and volume rates of flow, one with a smooth flat rigid bottom and the other containing the sand bed. Roughly, the difference in the two bottom drags, the one known, is equal to the difference in the net pressure forces on the water in the two channels, which is obtained from measurements of pressure differences across the partition at each end of the sand bed. Each experiment provides the drag, or average bottom stress, on the rippled sand bed as a function of the phase, θ, of the sinusoidal flow. From a first set of thirteen experiments with a medium sand, a stress coefficient, $f(\theta)$, is presented in three families of curves which explore the additional effects of flow velocity, ripple length, and deviations of the ripple profile from normal equilibrium. Average rates of energy dissipation are calculated. Results show f to be a complicated function of θ and other parameters. In particular, the instantaneous stress is not simply related to the instantaneous velocity. Some salient features of $f(\theta)$ are described, qualitatively, by a simple model.

I. INTRODUCTION

1. General

Water waves on the sea surface and sand ripples on the sea bed interact by processes of drag. Surface waves provide an oscillatory flow above the bed which produces and maintains bed forms by local movements of sand. The sand is scoured from the bed by tangential stresses under flows which include separation and vortex formation and which largely are shaped by the pressure field around the bed form. This field produces a distribution of normal stress over the surface of the bed. The horizontal force of these tangential and normal stresses on a large area of the bed, divided by that area, defines the average bottom stress. This is a function of time which becomes periodic as the bed forms become stable. When the bed form is two dimensional and periodic in space, the bottom stress is obtained by an average over a single ripple length. The reverse effect of the ripples on the surface waves is less direct and relatively minor, but is significant. The bottom stress combines with the oscillatory flow above the bed to dissipate energy. Ultimately, this energy is supplied by the surface waves which decay in the process. Also, the bottom stress is a factor in the refraction of surface waves. This paper describes laboratory measurements of bottom stress on naturally rippled sand beds as function of time.

2. Definition of Terms

Terms introduced in the preceding paragraph with others to be used in this study are defined by a few equations. Above the bed and beyond its effects the velocity of flow is

$$u_\infty = \left(\frac{2\pi a}{T}\right) \sin\left(\frac{2\pi t}{T}\right) = U \sin\theta \qquad (1)$$

where t is the time, T is the period and 2a is the orbital diameter of the water motion. Equation (1) defines the maximum velocity, U, and the phase, θ. The bed surface profile, assumed two dimensional and periodic with length λ, has elevation $h(x,\theta)$, where x is the horizontal coordinate. The average bottom stress is then defined by

$$\bar{\tau}(\theta) = \frac{1}{\lambda} \int_0^\lambda \left[\tau_h + (p_h - p_\infty)\frac{\partial h}{\partial x} \right] dx \qquad (2)$$

where τ_h is the local tangential stress on the bed, and $(p_h - p_\infty)$ is the difference between pressures at the bed surface and at any fixed elevation beyond the influence of the bed. Separate integrals for the two terms in the integrand would resolve $\bar{\tau}(\theta)$ into components expressing the effects of tangential and normal stresses, the latter being a form drag. However, such a separation is generally impossible. A stress coefficient,

$$f(\theta) = \frac{2\,\bar{\tau}(\theta)}{\rho U^2} \qquad (3)$$

where ρ is the density of the water, has been made dimensionless by dividing by ρU^2, rather than by $\rho u_\infty^2(\theta)$, in order to keep $f(\theta)$ proportional to $\bar{\tau}(\theta)$ throughout the cycle. The maximum of $f(\theta)$ is denoted f_m. The energy dissipated per unit area of bed per period, or twice that per half period, is given by

$$\Delta E = 2 \int_0^{T/2} \bar{\tau}\, u_\infty \, dt \qquad (4)$$

Then, inserting equations (1) and (3) into equation (4) and defining the average coefficient,

$$\bar{f}_1 = \frac{1}{\pi} \int_0^\pi f(\theta) \sin\theta \, d\theta \qquad (5)$$

produces,

$$\frac{\Delta E}{T} = \rho \frac{U^3}{2} \bar{f}_1 \qquad (6)$$

Thus, the rate of energy dissipation is proportional to $\bar{f}_1$.

3. Past Work

In the past, $f(\theta)$, f_m and $\bar{f}_1$ have been measured or estimated by various methods. These methods are here divided into two groups according to whether the surface of the bed was (1) artificially rigid or (2) naturally rippled.

(1) With rigid surfaces: Bagnold (1946) calculated $\bar{f}_1$ by the work needed to oscillate a metal cusp-shaped profile in still water. Kalkanis (1964) oscillated roughened plates in still water and observed flows which could be analyzed to provide $f(\theta)$. Using oscillatory-flow water tunnels, Jonsson and Carlsen (1976), in two experiments, measured velocity profiles over a flat roughened bed to obtain $f(\theta)$, while Kamphuis (1975) obtained f_m on a roughened shear plate in terms of relative grain roughness and a Reynolds number.

(2) With naturally rippled beds, $\bar{f}_1$ only has been obtained. By observation of the decay of surface waves, $\bar{f}_1$ has been calculated, in wave tanks, by Savage (1953) and by Inman and Bowen (1962) and, in field studies, by Bretschneider (1954) and by Iwagaki and Kakinuma (1967). Values of $\bar{f}_1$ from these field studies are summarized by Vitale (1979) and vary widely. Carstens, Neilson and Altinbilek (1969) measured the energy input required to maintain flows over sand beds in an oscillatory-flow tunnel restricted to a single period of 3.56 seconds and, within this limitation, presented $\bar{f}_1$ as function of grain size, D, and of a/D. Vitale (1979) has further analyzed and interpreted their results.

In sum, except with rigid flat roughened beds, measurements of bottom drag remain fragmentary. In particular, no previous measurements of $f(\theta)$ with naturally rippled beds have been reported.

4. Scope of the Present Study

To help fill this gap, the present study measures $f(\theta)$ in laboratory experiments with naturally rippled sand beds. Experiments are still in progress, but results from thirteen of them are presented, and preliminary conclusions are drawn. Values of $\bar{f}_1$ are calculated, and some features of $f(\theta)$ are discussed in terms of a simple model.

II. EQUIPMENT AND PROCEDURES

1. The Tunnel and its Modifications

The experiments are carried out in an oscillatory-flow water tunnel described by Lofquist (1977). Briefly, it is of U-tube design, and two tight fitting pistons in cylinders, side by side at one end, moving sinusoidally in unison, drive water back and forth through a horizontal test section and into and out of two reservoirs open to the air at the other end. The test section is 255 cm long, 21 cm wide, and has a mean depth of flow of 30 cm. The orbital diameter, 2a, and the period, T, can be selected arbitrarily below 250 cm and above, approximately, 1.5 seconds. Ranges in the present experiments are: $34.8 \text{ cm} < 2a < 76.6 \text{ cm}$, and $2.70 \text{ s} < T < 5.93 \text{ s}$.

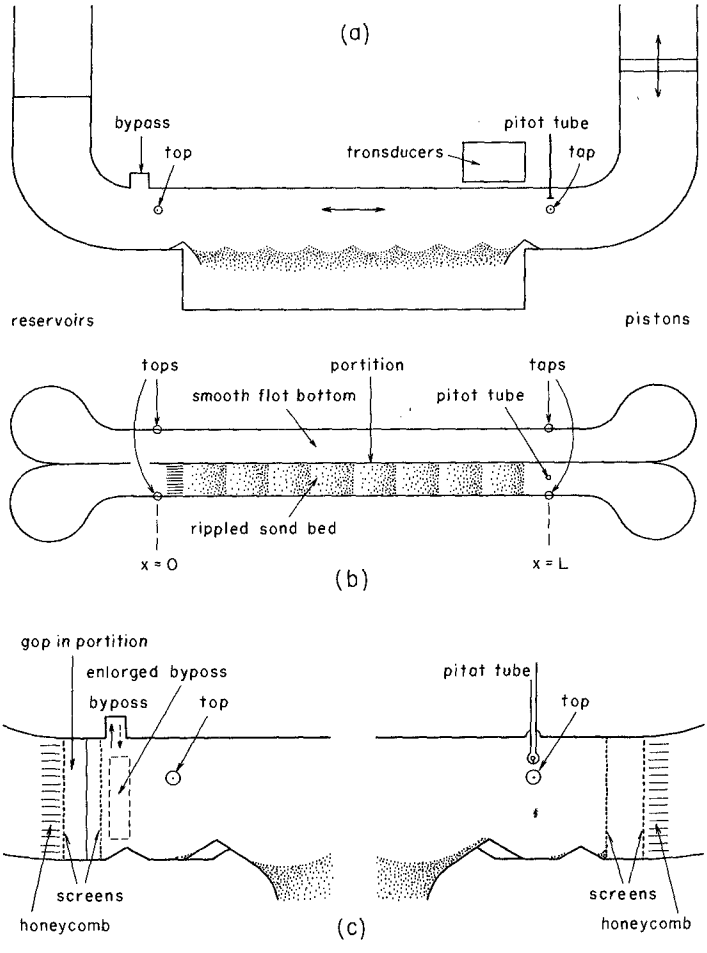

Figure 1. Schematic drawings of the tunnel and test section, (a) side view, (b) top view, (c) details of the two ends.

The tunnel has been modified for the present study as shown in the three schematic drawings of Figure 1(a),(b),(c). Of these, only (c) is drawn to scale. The channel has been split into two channels, each 10.1 cm wide, by a vertical partition (Fig.1,b). This partition separates each side from the other all the way from the pistons, at the right, to a point beyond the left end of the test section where the partition ends at a screen and there is a bypass over the channel top (Fig.1,c). (A screened bypass enlargement was cut in the partition just before the last three experiments.) One channel has a flat smooth metal bottom, while the other contains the rippled sand bed (Fig.1,b). In both channels, beyond the test section at either end, pressure taps have been mounted in the channel walls. These are indicated in all the drawings. A pitot tube has also been mounted which can be raised and lowered and which, with oppositely directed openings at its tip serving alternately as static and dynamic holes, can measure continuously the velocity of the reversing flow. The pressure taps in the walls and the pitot tube openings are connected to two differential pressure transducers which are located as indicated in Figure 1,(a). The connecting conduits are not shown. The purpose of these modifications will appear in the derivation of the stress measurement in section II,3 below.

2. End Conditions, Natural and Strained Profiles

The analysis in section II,3 requires that the areas of the four cross sections at the pressure taps be equal, so that migrations of the sand profiles into the conduits must be prevented. Therefore, rigid crest-shaped objects have been mounted at each end of the sand bed and, also, just before the first screens in order to stabilize the profiles and to keep the floor below the taps free of sand. These objects are shown in Figure 1,(c). The rigid crests at the ends of the bed are either of two sizes, selected best to match the sand crests between them. These rigid end crests condition the profiles since the number of sand ripple crests between them is some integer, M, and the fixed distance between them must equal $\lambda(M+1)$. Studies have shown (Lofquist, 1978, Fig. 22 and, more fully, Brebner, elsewhere in these proceedings) that an unconstrained two-dimensional profile adjusts λ/a to a natural value $(\lambda/a)_n$ which is a function of the degree of sand agitation and grain size but for low and moderate agitation is approximately equal to 1.33. Thus, in the tunnel, with λ and a selected such that $\lambda/a = (\lambda/a)_n$, the rigid end crests create minimum distortion of the sand profile between them.

With λ fixed by a selected number of sand ripple crests between the fixed end crests, it is possible, by varying a, deliberately to force λ/a away from $(\lambda/a)_n$ and so to produce a "strained" profile. Such profiles are described by Lofquist (1978), V,5. Briefly, as λ/a is reduced below 1.33, crests steepen and the profile appears "compressed" until at around $\lambda/a = 1.1$ somewhere a crest shrinks and disappears, and λ abruptly increases. As λ/a is increased above 1.33, crests flatten and the profile appears "extended", with low humps forming in the troughs, until at around $\lambda/a = 1.6$ one of these humps rises to become a new crest, and λ abruptly decreases. The deliberate variation of λ/a permits an investigation of the effect of profile strain on $f(\theta)$ and whether a natural profile gives $f(\theta)$ any special character.

3. Derivation of the Measurement of Stress

A simple analysis provides the average stress on the sand bed in terms of the pressures at the four taps and the velocity profiles measured by the pitot tube. Symbols used in the analysis are identified as applying either to the channel with the sand bed or with the smooth bottom by a subscript "s" or "o" respectively. These symbols are: L, H and b, the length, depth and width of the channels (the same for each); p(0) and p(L), the pressures at the taps at x = 0 and L; $\bar{\tau}$ and $\bar{\tau}_p$, the average stresses on the bottom and on the smooth perimeter of the walls and top; Q, the volume rate of flow; $\overline{u^2}$, the average of u^2 over a cross section, where u is the local velocity.

Then, by momentum balance in each of the channels,

$$bH\,[p(0)-p(L)]_s - bL\,\bar{\tau}_s - L(2H+b)\,\bar{\tau}_{ps} = \rho L\dot{Q}_s + \rho bH\,[\overline{u^2}(L)-\overline{u^2}(0)]_s \qquad (7)$$

and

$$bH\,[p(0)-p(L)]_o - bL\,\bar{\tau}_o - L(2H+b)\,\bar{\tau}_{po} = \rho L\dot{Q}_o + \rho bH\,[\overline{u^2}(L)-\overline{u^2}(0)]_o \qquad (8)$$

where a dot denotes a derivative with respect to time. Since $\dot{Q}_s$ is known and $\bar{\tau}_{ps}$ can be estimated, $\bar{\tau}_s$ can, in principle, be determined by equation (7). This approach was attempted before the channel was divided. But each side of equation (7) is dominated by its first term, and $L\bar{\tau}_s$ is easily obscured by noise and scatter in measurements of $H[p(0)-p(L)]_s$. Instead, equation (7) is subtracted from equation (8). In doing so, $\dot{Q}_o - \dot{Q}_s$ vanishes, since Q_o and Q_s are made equal by construction of the tunnel with two pistons of equal area. Also, $\bar{\tau}_{ps} - \bar{\tau}_{po}$ can be discarded, since the terms are of nearly equal magnitude and each, as estimated by laminar theory, is small compared with $\bar{\tau}_s$ as eventually determined. Finally, since the development of the velocity profile over the smooth bottom is relatively small, the last term in equation (8) can be discarded. The subtraction then provides,

$$\bar{\tau}_s - \bar{\tau}_o = \frac{H}{L}\,[(p_o-p_s)_L - (p_o-p_s)_0] - \frac{\rho H}{L}\,[\overline{u_s^2}(L)-\overline{u_s^2}(0)] \qquad (9)$$

where the pressure differences are between pairs of taps at x = L,0.

With $\bar{\tau}_o$ calculated by laminar theory, results of the experiments eventually show that $\bar{\tau}_s$ dominates the left side of equation (9) and that the right side is dominated by the first pressure difference, with the second kept relatively small by the action of the by-pass. The last term, which, like $\bar{\tau}_o$, proves to be small compared with $\bar{\tau}_s$, is provided by the single pitot tube at x = L with the assumption that, with z the vertical coordinate, $u_s(x,z,\theta)$ satisfies the condition of symmetry,

$$u_s(0,z,\theta) = -\,u_s(L,z,\theta\pm\pi) \qquad (10)$$

4. Pressure Measurement

A differential pressure transducer mounted over the test section near the taps at x = L (Fig.1,a) is alternately connected with the two pairs of taps at x = 0,L by suitable conduits and valves (not shown in the drawings). Next to it is mounted a second pressure transducer connected with the pitot tube. Signals from the transducers are recorded on paper tape as functions of time. Pen deflections, in mm, are translated into pressure units by a calibration in which, immediately following an experiment, a simple device provides selected hydrostatic pressure differences to a transducer while the recorder runs with the same amplification as before.

Filters are required to reduce noise in the transducer output signals. These filters consist of six sand-filled glass loops one of which is included in each of the conduits between the transducers and the four pressure taps and the two pitot tube openings. This filtering reduces the amplitude and slows the response of the output signal. These distortions must be removed by calibration of another type. With the pressure at one tap, or pitot opening, fixed by draining the water in the tank to the level of an open hatch, the other is connected by a flexible tube to a vessel which is filled with water to this same level. The vessel is then oscillated vertically in simple harmonic motion with selected amplitude, h_c, and period, T_c, to supply a known (non hydrostatic) sinusoidal pressure difference to the transducer. Denoting, for given h_c, the ratio of the amplitude of the output signal as $T_c \to \infty$ to that at T_c by Φ, and the phase lag by ϕ, calibrations are obtained in the form,

$$T_c^2 \, (\Phi^2-1) = F_1(T_c) \tag{11}$$

and

$$T_c \tan \phi = F_2(T_c) \tag{12}$$

where F_1 and F_2 are independent of h_c and are slowly varying functions of T_c or constant. Although subject to adjustments and slight drift over long periods of time, representative constant average values for both pairs of taps are, $F_1 \simeq 4.3$ sec^2, $F_2 \simeq 2.5$ sec, and for the pitot tube, $F_1 \simeq 9.7$ sec^2, $F_2 \simeq 4.3$ sec.

5. Processing the Data

As the first term on the right side of equation (9) has been found to dominate the last term, the processing of records from the pressure taps has differed from that of records from the pitot tube and will be considered first. The primary records from the pairs of taps at x = 0,L are the pen deflections, in mm, which are denoted $P(0,\theta)$ and $P(L,\theta)$ respectively. Figure 2 shows $P(L,\theta)$ and $P(0,\theta)$ for a typical experiment (no. 2 in Table 1 below). In each case residual noise has been averaged out to produce a smoother curve. The deflections of $P(0,\theta)$ are kept relatively small by the action of the by-pass. The phase is marked for $\theta = 0, \pi, 2\pi$. A digitizing pad, or table, reads the analog tape records at each

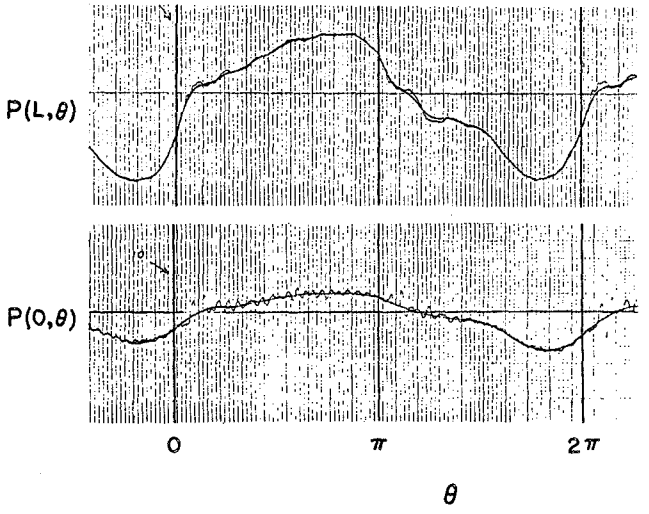

Figure 2. A typical record of transducer output from the two pairs of pressure taps.

10 degrees of phase and stores the data in a microcomputer. The computer then processes the data in the following steps:

(1) As required in equation (9), the difference in the records is taken to form

$$D(\theta) = P(L,\theta) - P(0,\theta) \tag{13}$$

(2) Ideally, the stress at any time should be the negative of that a half cycle earlier or later in the opposite direction, so that $D(\theta)$ should equal $-D(\theta \pm \pi)$. This condition is only approximately realized. Therefore, $D(\theta)$ is averaged with $-D(\theta + \pi)$ to produce the function

$$\overline{D}(\theta) = \frac{1}{2}[D(\theta) - D(\theta + \pi)] \tag{14}$$

which changes only in sign when advanced a half cycle. In Figure 3 below, for each of the thirteen experiments, points giving $D(\theta)$ and $-D(\theta + \pi)$ are plotted at each 10 degrees of phase, and $\overline{D}(\theta)$ is shown.

(3) $\bar{D}(\theta)$ is resolved into a sum of sinusoidal components by Fourier analysis. Both sine and cosine terms are present with arguments $n\theta$, where n, an integer, is the number of the harmonic, but since $\bar{D}(\theta) = -\bar{D}(\theta + \pi)$, even harmonics are absent, and n is odd.

(4) Successively taking $T_c = T/n$, the calibration corrections for the filter distortions given by equations (11),(12) are applied to each component, and

(5) The series is reassembled to provide a corrected $\bar{D}(\theta)$. This reassembly has included terms as far as the 7th harmonic while checking that the increment from the 9th harmonic is insignificant.

(6) By use of the hydrostatic pressure calibrations, $\bar{D}(\theta)$ is expressed in pressure units to provide the first term on the right side of equation (9).

The records from the pitot tube, also contained on the paper tapes, have been processed manually, without computer or Fourier analysis. The last term in equation (9) has been approximated using overall filter corrections, those provided by equations (11) and (12) for n = 1. Errors associated with this approximation cannot be serious, since this term has been found to be small, its range less than 8%, and typically less than 5%, of the main term.

The remaining unknown term in equation (9), $\bar{\tau}_o$, is calculated by the theory for laminar oscillatory flow over a plane surface. Its range has proven to be less than 3% of that of $\bar{\tau}_s$.

IV. RESULTS

1. Summary of Experiments

The major results of this paper are curves of f as function of θ and of the parameters U, λ, λ/a from the thirteen experiments analyzed so far. In Table 1 these experiments are identified by number, in chronological sequence, and by values of their parameters M, λ, a, U, and including the redundant $T = 2\pi a/U$. The trough to crest ripple height, η, has also been added (except where the record remains on undeveloped film). M is the number of sand crests between the fixed end crests and determines λ, as described in section II,2. Experiments for which λ/a differs from $(\lambda/a)_n$, that is, those with strained profiles (sec.II,2), are denoted by asterisks. Experiment "C" is a composite of nos. 2 and 26 as described in section IV,2. All thirteen experiments have used quartz sand with $D_{50} = 0.55$ mm.

Table 1. Parameters for the Thirteen Experiments

D_{50} = 0.55 mm

Exp. no.	M	λ,cm	a,cm	U,cm/s	T,s	η,cm
1	7	31.8	23.9	27.0	5.57	7.3
2	7	31.8	23.9	40.6	3.71	6.9
3	7	31.8	23.9	33.1	4.55	7.8
4*	7	31.8	25.5	33.3	4.83	7.2
5*	7	31.8	21.9	33.1	4.16	6.7
6*	7	31.8	20.6	33.15	3.90	5.7
7*	7	31.8	27.7	33.2	5.25	7.6
13	10	23.1	17.4	40.5	2.70	4.8
18	5	43.5	31.9	40.6	4.94	9.3
24	4	52.5	38.3	40.6	5.93	11.9
26	7	31.8	23.9	40.5	3.72	-
27	7	31.8	25.9	52.I	3.13	-
28	7	31.8	28.9	63.6	2.86	-
C	7	31.8	23.9	40.5	3.71	-

*With strained profiles, $\lambda/a \neq (\lambda/a)_n$

2. Reliability

Interpretation of the results to follow requires some assessment of their reliability. The most convenient measure of reliability is the extent to which the stress, and related measurements, change only in sign as θ is increased by π, that is, the agreement between $D(\theta)$ and $-D(\theta + \pi)$ defined in sec.II,5 and by equation (13). In Figure 3, $D(\theta)$, $-D(\theta + \pi)$ and their average $\bar{D}(\theta)$ (eq. 14) are shown for each experiment, identified by its number in Table 1. The scales of $D(\theta)$ and $-D(\theta + \pi)$, are in tape units before calibration and are of no interest beyond the indicated zero marks. Discrepancies between $D(\theta)$ and $-D(\theta + \pi)$ remain within 10% for the most part but are occasionally considerably larger. Their cause is unknown. They are most plausibly associated with pressure buildups behind the screens and resulting

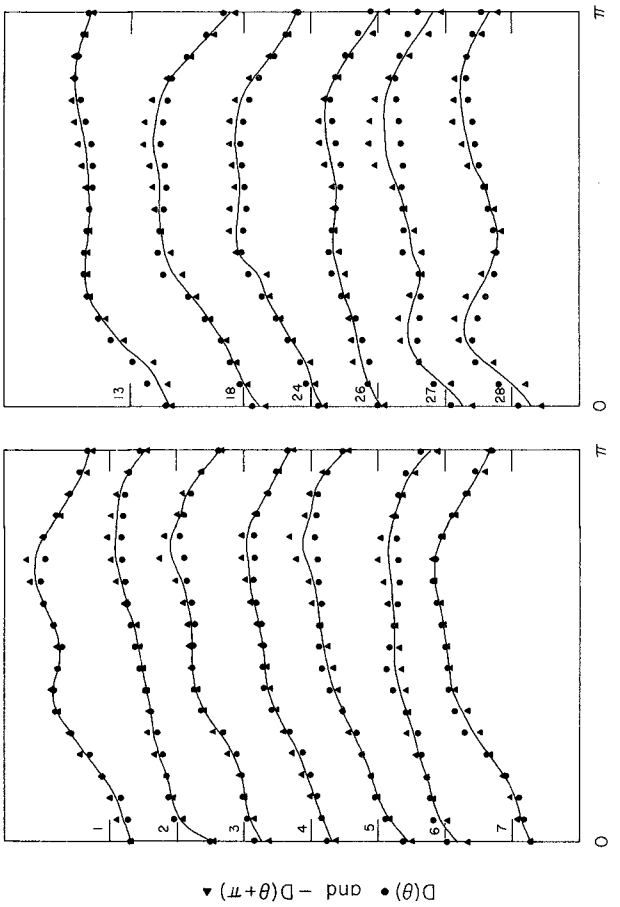

Figure 3. Applying the condition of symmetry between flows left to right, D(θ), and right to left, −D(θ+π). Experiments are numbered as in Table 1.

flows through the by-pass. Pressure buildups are caused especially by sand in suspension being carried to and accumulating against a screen during a part of the cycle and become large enough to require limitations on U in order to forestall damage to the screens. The discrepancies may, in part, also derive from slight asymmetries in the sand profiles from one end of the bed to the other, particularly near the fixed end crests. Whatever their cause, such discrepancies reduce confidence in an experiment and if too large may cause it to be discarded.

Three of the experiments, nos. 26,27,28, were performed (after the oral presentation) following an enlargement of the by-pass to reduce the pressure difference $(p_o - p_s)_0$ (eq. 9) especially at higher values of U. Except for this enlargement, exps. 2 and 26 are ostensibly the same, and have been combined into a composite experiment numbered "C". Figure 4 shows $f(\theta)$ for exps. 2, 26, and "C". These curves agree reasonably well over most of the range but diverge substantially near times of flow reversal. Exps. 27 and 28 replace two experiments, included in the oral presentation, which had the same values of U, but had $\lambda/a = 1.33$, rather than $(\lambda/a)_n$ as in exps. 27 and 28. At these high values of U, $(\lambda/a)_n$ is significantly less than 1.33. In these two earlier experiments, ranges of $P(0,\theta)$ exceeded one half those of $P(L,\theta)$ and discrepancies between $D(\theta)$ and $-D(\theta + \pi)$ were substantially larger than in exps. 27 and 28, and, perhaps in consequence, their curves of $f(\theta)$ were quite different.

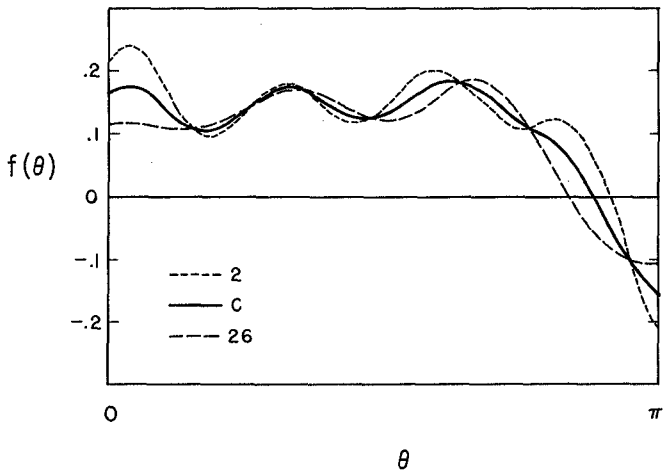

Figure 4. $f(\theta)$ for experiments 2 and 26 and their composite "C".

3. The Curves of $f(\theta)$

The curves of $f(\theta)$ from the twelve experiments (after combining nos. 2 and 26), for selected parameters, are shown in Figures 5,6,7. In Figures 5 and 6 the profiles are natural, with $\lambda/a = (\lambda/a)_n$, and in Figure 7 they are strained. $(\lambda/a)_n = 1.33$ in all experiments except nos. 27 and 28, in Figure 5, where it is reduced by the large values of U. In each figure, or family, the curves are identified at their left by their numbers in Table 1 and are arranged in order of monotonic increase or decrease in the defining parameter. In Figures 5 and 6 this parameter is U and λ, respectively, and in Figure 7 it is λ/a. The numerical value of the varying parameter is given at the right of each curve, and conditions and values of parameters held constant are shown above each family or figure. Although $f(\theta)$ is determined by its behavior over the restricted range $o < \theta < \pi$, since $f(\theta + \pi) = - f(\theta)$, it is here presented over the entire cycle $-\pi/2 < \theta < 3\pi/2$ so that features of $f(\theta)$, such as maxima and minima, can more easily be followed from one curve to the next as the parameter is varied.

4. Values of $\overline{f}_1$ and f_m

With equation (5), values of $\overline{f}_1$, the measure of energy dissipation, have been calculated from the twelve curves of $f(\theta)$ already presented. Table 2 lists these values in the same order as the curves in Figures 5, 6,7. For comparison, maximum values of $f(\theta)$, f_m, have been included.

Table 2. Values of $\overline{f}_1$, proportional to the rate of energy dissipation, and f_m for the curves in Figures 5,6,7.

Natural profiles						Strained profiles		
λ = 31.8 cm			U ≃ 40.6 cm/s			λ = 31.8 cm U ≃ 33.2 cm/s		
U,cm/s	$\overline{f}_1$	f_m	λ,cm	$\overline{f}_1$	f_m	λ/a	$\overline{f}_1$	f_m
27.0	.122	.299	52.2	.129	.282	1.15	.113	.253
33.1	.102	.236	43.5	.115	.259	1.25	.105	.228
40.5	.083	.180	31.8	.083	.180	1.33	.102	.236
52.1	.075	.218	23.1	.115	.452	1.45	.107	.228
63.6	.072	.348				1.54	.086	.227

The combination U = 40.6 cm/s and a = 23.0 cm occurs in the observations of Carstens, Neilson and Altinbilek (1969) where T = 3.56s. At this value of a and with D = 0.585 mm, curves in their Figures 11 and 23 give $\lambda \simeq 27.0$ cm and $\overline{f}_1 \simeq .111$ (with their $\overline{f}$ replaced by $3\pi\overline{f}_1$).

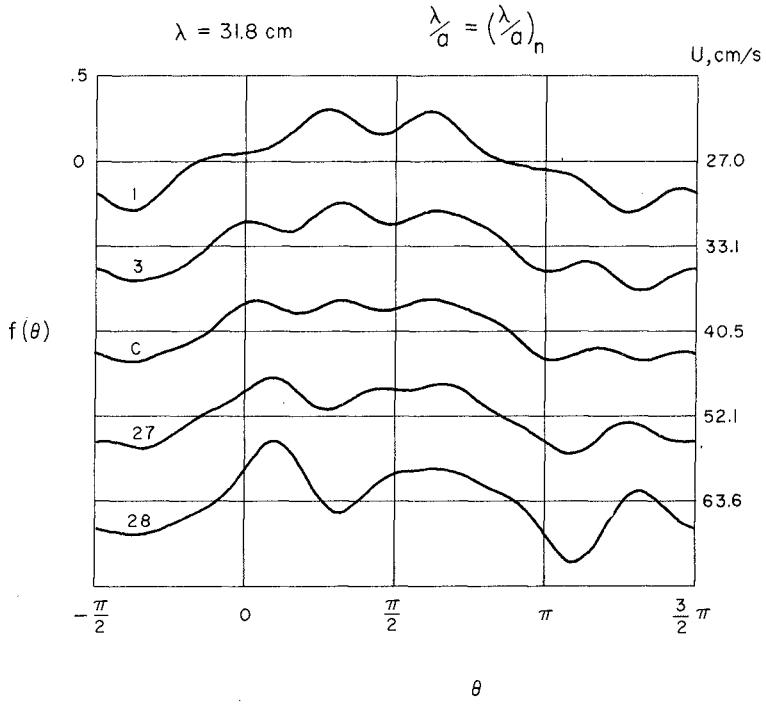

Figure 5. Stress coefficient f as function of phase θ and velocity U, for natural profiles.

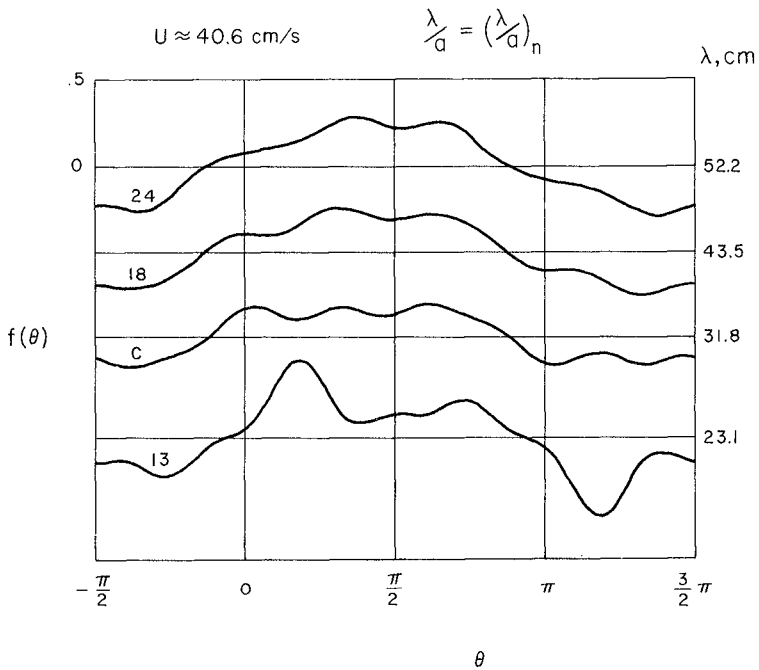

Figure 6. Stress coefficient f as function of phase θ and ripple length λ, for natural profiles.

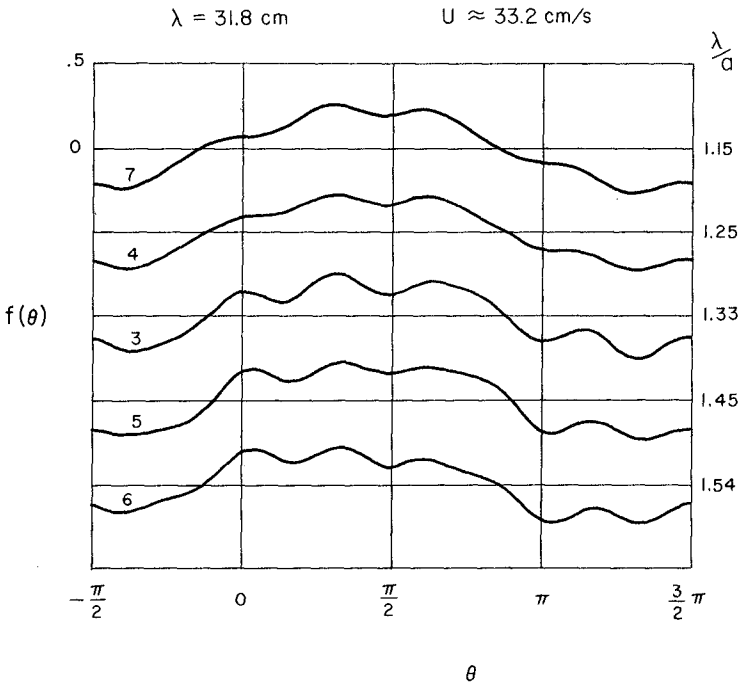

Figure 7. Stress coefficient f as function of phase θ and λ/a, for strained profiles.

IV. DISCUSSION

1. Conclusions Regarding $f(\theta)$ and $\bar{f}_1$.

Defined by the magnitude, shape and phase of their peaks and valleys, the character of the curves in Figures 5,6,7 is found to progress continuously from one to the next as, within each family, U, λ and λ/a take on successive values. This continuity supports the reliability of the curves at hand, some of which will be repeated for further confirmation. Although restricted in the ranges of their parameters, the curves obtained permit some preliminary conclusions to be drawn. It is to be remembered that $u_\infty(\theta) = U \sin \theta$, as in equation (1).

The shapes of the functions $f(\theta)$ in Figures 5,6,7 differ markedly for different values of the parameters. Therefore, there can exist no "universal" function $f(\theta)$ to which all curves can be reduced by a selection of scale. In particular, in no case has $f(\theta)$ been found to be proportional to $\sin^2\theta$. Thus, the instantaneous stress is not, in general, proportional to the square of the instantaneous velocity.

The values of $\bar{f}_1$ listed in Table 2 are found to vary smoothly with their parameters and, so far, to be fairly constant. In contrast, f_m, which is also listed, varies more abruptly and does not remain proportional to $\bar{f}_1$. Thus, f_m does not provide a reliable measure of the rate of energy dissipation.

2. No Effect of Strain

It might be supposed that as a developing profile approaches equilibrium, or as a strained profile approaches an unstrained "natural" condition, the stress would take on some special stationary character, expressing, in some form, the principle of least action. However, the curves of $f(\theta)$ in Figure 7 and the values of $\bar{f}_1$ in Table 2 vary continuously with λ/a, with no discernible special character or extremum at $\lambda/a = 1.33$ where the profile is unstrained or natural. The ripple profiles of Figure 7, though strained, are stable, and these experiments have not examined the stress on unstable profiles during times of growth or change.

3. A Simple Model

Certain features common to all the curves of $f(\theta)$ in Figures 5,6,7 suggest a general, though limited, interpretation in terms of a simplified physical model. These features are three: (1) a positive stress at $\theta = 0$, (2) one or two peaks in $f(\theta)$ in the range $0 \leq \theta < \pi/2$, and (3) a single peak in $f(\theta)$ in the range $\pi/2 < \theta < \pi$. It is first recalled that the stress on a rigid flat bed precedes $u_\infty(\theta)$ by a shift in phase which is a maximum, $\pi/4$, for a smooth bed with laminar flow and stress and decreases as the bed becomes more rough and the stress more turbulent. Thus, with $u_\infty(\theta) = U \sin \theta$ such a stress would have a maximum in the range $\pi/4 < \theta < \pi/2$. The model simply combines such a "flat-bed stress" on the upstream face of the ripple crest with the stresses of vortex action, which is essential to ripple equilibrium.

The process of vortex formation and action adopted by the model is familiar. Following flow reversal, tangential stress on the upstream ripple face generates a boundary-vorticity layer and sets sand into motion, skewing the crest to end abruptly in a steep lee slope and sliding and spilling into the trough. The sharp curvature of the crest enhances separation of flow, and, as it is carried past, the boundary layer, with its vorticity, detaches and rolls into a vortex, still spilling sand into the trough. The center of the vortex is slowed and then held over the trough by reduced pressure on the lee slope of the crest, creating a form drag. Around the time of the succeeding flow reversal, the spinning vortex sweeps sand out of the trough and back up or over the crest, thus maintaining the profile.

Returning to $\theta = 0$, the spin of the vortex formed during the preceding half cycle and centered over the trough contributes a positive stress, while pressures needed to hold the vortex in position vanish at about this time. Thus, $f(0) > 0$. Following flow reversal, the vortex, decaying but still spinning, is carried up the ripple face where its spin hastens and increases the stress. Spin decay and the rapid drop off in spin stress as the vortex passes the ripple crest can account for an early maximum of the spin stress, slightly before or after $\theta = 0$, and preceding the maximum of the flat-bed stress. Thus, depending upon the relative strengths of these two maxima and their separation in time, $f(\theta)$ can display one or two peaks in the range $0 < \theta < \pi/2$. The deceleration of the forming vortex (or, more accurately, of several small vortices which later amalgamate) by reduced pressure on the lee slope begins with flow separation soon after flow reversal, but the associated form drag reaches a single peak as the vortex approaches full development sometime in the range $\pi/2 < \theta < \pi$, when the flat-bed stress is in decline. A negative back-flow stress on the lee ripple slope and under the vortex accompanies this form drag, and develops to make $f(\pi) < 0$ as the form drag vanishes.

The value of $\overline{f}_1$ from Carstens, Neilson and Altinbilek (1969), noted in section III, 4 above, fits well with values listed in Table 2. However, in Figures 5,6,7 the peaks in $f(\theta)$ preceding and nearest $\theta = \pi/2$, which the model associates with the flat-bed stress, are an order of magnitude larger than values of f_m obtained by Kamphuis (1975) at the same values of a/D and aU/ν. At least to some extent, this large increase may be a result of the movement of sand grains on the ripple face (cf. Lofquist in discussion of Vitale, 1979). Similarly, the peaks in $f(\theta)$ following $\theta = \pi/2$, which the model associates with form drag and vortex formation, suggest a form drag contribution to $\overline{f}_1$ of, roughly, one third. This is several times the seven percent which Tunstall and Inman (1975) have estimated for the ratio of vortex energy to the total energy dissipated in a half cycle. Their estimate was based upon a study of vortex formation behind rounded rigid (lithified) ripple crests. Possibly, the relative sharpness of a naturally skewing crest substantially enhances flow separation and vortex formation, or, the vortex energy is only a part of the form drag contribution to $\overline{f}_1$.

4. Limitations and a Correction

Whatever its merits, the model is severely limited. Processes which interact cannot simply be added as flat-bed and vortex stresses. Concentration of all the vorticity generated on the upstream face of a crest into a single vortex formed in its lee is not a universal mechanism. In particular, at higher rates of flow, and scour, the ripple crests become lower and closer and unable to form and hold vortices large enough to contain all the detached boundary layer, and flow patterns modify. Such appeared to be the case with exp. 28.

When large quantities of sand are set in motion, $f(\theta)$ as calculated by equation (9) itself loses precision and requires the addition of a correction, $\Delta f(\theta)$. If, at any θ, the sand in motion lowers the mean surface by Δh (a positive quantity) and has a momentum m_s per unit area of the bed, and with $Q_s = bHU \sin \theta$, a rederivation of $f(\theta)$ produces the correction term

$$\Delta f(\theta) = \frac{2\Delta h}{a} \cos \theta - \frac{2}{\rho U^2} \dot{m}_s \qquad (15)$$

In experiment 28, Figure 5 shows $f(\theta)$, surprisingly, to be negative in the neighborhood of $\theta = \pi/3$. Here, $\Delta h \cos \theta$ is positive while $\dot{m}_s$ is presumably negative, as sand scoured from the bed during the preceding peak in $f(\theta)$ falls back to impact the bed and lose its momentum. Thus, $\Delta f(\theta)$ is presumably positive and, while its magnitude can only be guessed at, it could suffice to keep the corrected $f(\theta)$ positive.

5. Future Work

The experiments described here are part of a larger program interrupted by the timing of the conference. As noted above, future experiments will investigate the repeatability of present results, and will extend the ranges and the number of combinations of the parameters. One or two finer sands will be included. Future more complete analyses will more consistently combine parameters into dimensionless ratios. A completed study is scheduled for publication in 1981 by the Coastal Engineering Research Center, Ft. Belvoir, Virginia.

ACKNOWLEDGEMENT

The results presented in this paper are based on research conducted at the National Bureau of Standards. This research is wholly supported by the Coastal Engineering Research Center under the Beach Behavior and Restoration Research Program of the U.S. Army Corps of Engineers. The findings reported here are not to be construed as an official Department of the Army position unless so designated by other authorized documents. Permission to publish this information is appreciated.

REFERENCES

BAGNOLD, R.A., "Motion of Waves in Shallow Water, Interaction Between Waves and Sand Bottoms," Proc. Roy. Soc. London, Ser. A, Vol. 187, 1946, pp. 1-18.

BRETSCHNEIDER, C.L., "Field Investigation of Wave Energy Loss of Shallow Water Ocean Waves," TM-46, U.S. Army Corps of Eng., BEB, Sept. 1954.

CARSTENS, M.R., NEILSON, F.M., and ALTINBILEK, H.D., "Bed Forms Generated in the Laboratory Under and Oscillatory Flow: Analytical and Experimental Study," TM-28, U.S. Army Corps of Eng., CERC, June 1969.

INMAN, D.L., and BOWEN, A.J., "Flume Experiments on Sand Transport by Waves and Currents," Proc. Eighth Coastal Eng. Conf., 1962, pp. 137-150.

IWAGAKI, Y., and KAKINUMA, T., "On the Bottom Friction Factors Off Five Japanese Coasts," Coastal Eng. in Japan, Vol. 10, 1967, pp. 13-22.

JONSSON, I.G., and CARLSEN, N.A., "Experimental and Theoretical Investigations in an Oscillatory Turbulent Boundary Layer," Journal Hyd. Res. Vol. 14, No. 1, (1976), pp. 45-60.

KALKANIS, G., "Transportation of Bed Material Due to Wave Action," TM-2, U.S. Army Corps of Eng., CERC, Feb. 1964.

KAMPHUIS, J.W., "Friction Factors Under Oscillatory Waves," Jour. Waterways, Harbors and Coastal Eng. Div., ASCE, Vol. 101, No. WW2, May 1974, pp. 135-144.

LOFQUIST, K.E.B., "A Positive Displacement Oscillatory Water Tunnel," MR 77-1, U.S. Army Corps of Eng., CERC, Feb. 1977.

LOFQUIST, K.E.B., "Sand Ripple Growth in an Oscillatory-Flow Water Tunnel," TP 78-5, U.S. Army Corps of Eng., CERC, Aug. 1978.

SAVAGE, R.P., "Laboratory Study of Wave Energy Losses by Bottom Friction and Percolation," TM-31, U.S. Army Corps of Eng., BEB, Feb. 1953.

TUNSTALL, E.B., and INMAN, D.L., "Vortex Generation by Oscillatory Flow Over Rippled Surfaces," Journal of Ceophysical Research, Vol. 80, No. 24, Aug. 1975, pp. 3475-3484.

VITALE, P., "Sand Bed Friction Factors for Oscillatory Flows," Journal of the Waterway, Port, Coastal and Ocean Div., Proc. ASCE, Vol. 105, No. WW3, Aug. 1979, pp. 229-245.

Contribution to the Discussion During Session C,
Coastal Processes, Friday, March 28, 2:00 p.m.

by

M. S. Longuet-Higgins
Institute of Oceanographic Sciences
Wormley, Surrey, England

Professor Brebner suggested that the profile of sand ripples should be approximated by a conformal transformation into a hexagon, as has been done for steep surface waves (Longuet-Higgins, 1973). In fact the ripple profile is often steeper than this, the angle at the crest being closer to 108° (the interior angle of a pentagon) than to 120°. See, for example, the experimental data summarized by Nielsen (1979), Figures 5.7 to 5.11. For the pentagon approximation, the ratio of ripple height to ripple wavelength would be

$$\frac{H}{L} = \frac{\ln \sec \pi/5}{2\pi/5} = 0.169 \ .$$

In fact polygons with any number P of sides may be used, and we may extend the analysis to all rational values P = N/M by considering polygons enclosing their centre M times.

The great advantage of the polygon approximation is that the flow outside the polygon (i.e., above the ripple) may be quite simply mapped onto the interior of a circle. Irrotational flow over the ripple is represented by a simple vortex at the center of the circle. Any other vorticity shed by boundary layers at the crests can be represented by point-vortices and their images in the circle.

Calculations using these ideas are at present in hand (Longuet-Higgins, 1980 a,b). It has already been shown that they yield drag coefficients in excellent agreement with those measured by Bagnold (1946) and by Carstens, et al. (1969).

References

Bagnold, R.A. 1946 Proc. R. Soc. Lond. A 187, 1-15.

Carstens, M.R. Nielson, F.M. and Altenbilek, H.D. 1969. C.E.R.C. Tech. Mem. No. 28, 78 pp.

Longuet-Higgins, M.S. 1973. Proc. R. Soc. Lond. A 331, 445-465.

Longuet-Higgins, M.S. 1980a. "Polygon transformations in fluid mechanics." Proc. 7th Int. Conf. on Numerical Methods in Fluid Mechanics, Stanford, Calfiornia, June 1980.

Longuet-Higgins, M.S. 1980 b "Oscillating flow over steep sand ripples." Submitted to J. Fluid Mech.

Nielsen, P. 1979. I.S.V.A., Tech. Univ. of Denmark, Lyngby, Series Pap. No. 20, 160 pp.